

Experimental assessment of PIV/PTV-based pressure reconstruction techniques applied to a low-speed base flow

van Gent, Paul; Gentile, Valeria; van Oudheusden, Bas; Schrijer, Ferdinand

Publication date

2016

Document Version

Accepted author manuscript

Published in

Proceedings of the International Workshop on Non-Intrusive Optical Flow Diagnostic

Citation (APA)

van Gent, P., Gentile, V., van Oudheusden, B., & Schrijer, F. (2016). Experimental assessment of PIV/PTV-based pressure reconstruction techniques applied to a low-speed base flow. In *Proceedings of the International Workshop on Non-Intrusive Optical Flow Diagnostic: Delft, The Netherlands*

Important note

To cite this publication, please use the final published version (if applicable).
Please check the document version above.

Copyright

Other than for strictly personal use, it is not permitted to download, forward or distribute the text or part of it, without the consent of the author(s) and/or copyright holder(s), unless the work is under an open content license such as Creative Commons.

Takedown policy

Please contact us and provide details if you believe this document breaches copyrights.
We will remove access to the work immediately and investigate your claim.

Experimental assessment of PIV/PTV-based pressure reconstruction techniques applied to a low-speed base flow

P.L. van Gent, V. Gentile, B.W. van Oudheusden and F.F.J. Schrijer

Delft University of Technology, Faculty of Aerospace Engineering, The Netherlands

1. Introduction

Quantification of surface pressure is critical for the efficient design of aerospace structures. One way of measuring pressure is PIV/PTV-based pressure reconstruction [1]. In this approach, PIV/PTV data are used to determine the material acceleration and subsequently pressure via the momentum equation. In recent years, the technique has become increasingly feasible and appealing due to the development of (time-resolved) volumetric diagnostic capabilities, such as tomographic PIV [2] and Lagrangian particle tracking [3]. The performance of a variety of state-of-the-art techniques was recently assessed for the case of a transonic base flow within the collaborative European framework programs 'NIOPLEX' [4]. Since the NIOPLEX test case considers a simulated experiment, it does not necessarily demonstrate the actual capabilities of PIV/PTV-based pressure reconstruction techniques for realistic measurement conditions.

The present study overcomes this limitation by reconstructing pressure from actual PIV/PTV measurements of a flow that is similar to the NIOPLEX test case, i.e. an axisymmetric step albeit in a low-speed flow, facilitating comparison. Reference measurements are obtained using microphones and static pressure sensors to provide a source for comparison.

2. Experimental arrangements and measurement techniques

Measurements were conducted in the low-speed wind tunnel (W-Tunnel) of the Aerodynamics Laboratories of Delft University of Technology. The freestream velocity (U_∞) of the flow is 10 m/s and the Reynolds number based on the model diameter (Re_D) is about 35,000.

The model is an ogive-cylinder with a diameter (D) of 50 mm equipped with an afterbody with a diameter of 20 mm (0.4 D) and a length of 90 mm (i.e. 1.8 D). (see Fig. 1). The afterbody contains pinholes with a spacing of 10 mm (0.2 D) for measurements of pressure fluctuations via microphones and of the mean pressure using static pressure ports. The model is supported by a wing-shaped airfoil (NACA 0018, 60 mm chord length).

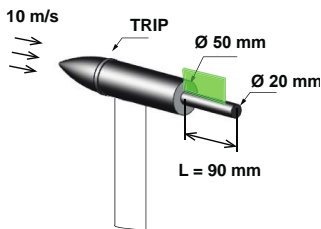


Fig. 1. Wind-tunnel model

PIV measurements are performed in a thin volume located downstream of the step above the pinholes (see Fig. 1). The size of the measurement volume is $1.5D \times 0.7D \times 0.07D$ ($75 \text{ mm} \times 35 \text{ mm} \times 3.5 \text{ mm}$, $L \times H \times W$). The flow uniformly seeded by a SAFEX smoke generator with particles of $1 \mu\text{m}$. The typical seeding concentration is 0.05 particles per pixel (ppp). Particles are illuminated by a Quantronix Darwin Duo Nd-YLF laser ($2 \times 25 \text{ mJ/pulse}$ at 1 kHz). Particle images are recorded by four Photron FastCAM SA1.1 CMOS cameras (maximum resolution 1024×1024 pixels, $20 \mu\text{m}$ pixel pitch) placed at opposite sides of the test section. All cameras are placed at a yaw angle of

about 30° to receive forward scattered light. Two cameras, equipped with a 60 mm Nikon objectives, are located at the same height as the base of the model at either side of the field of view. The two other cameras are placed to view from above at a pitch angle of about 40° . These cameras are equipped with 105 mm Nikon objective. The aperture is set to $f_\# = 5.6$. The magnification is 0.25 and the resulting digital resolution is $12.3 \text{ pixel mm}^{-1}$.

Images of 1024 x 512 pixels are recorded at 10 kHz in single-frame mode, leading to a time separation of 100 μ s, corresponding to a maximum particle displacement of 12 pixels. The recordings consist of 10,941 images over a time span of about 1.1 second.

Particle images are enhanced by subtracting the local minimum intensity over a 101 image-sized kernel and subtracting the minimum intensity within 31 voxel-sized kernels. The resulting intensity is normalised by a min-max filter with a kernel of 6 voxels. Gaussian smoothing and sharpening is applied to obtained more better defined particles. This approach was empirically found to reduce the number of outliers in the velocity fields obtained after further processing. The resulting particle image size is about 2.5 pixels, leading to a source density (N_s) of about 0.25.

After volume self-calibration [5], reconstructed volumes are obtained by 25 iterations of the SMART algorithm after initialisation by the MLOS algorithm [6]. $3 \times 3 \times 3$ Gaussian smoothing applied after each iteration, excluding the final iteration. Voxels with intensities below 0.01 counts are not updated. The resulting reconstructions have a signal-to-noise ratio (SNR) of about 5.

Cross-correlation analysis is performed using 2 consecutive particle volumes as well as using 9 consecutive volumes with the fluid trajectory correlation algorithm (FTC [7]). All correlation analyses employ iterative multi-grid volume deformation (VODIM, based on [8]), symmetric block direct correlation [9] and Gaussian volume weighting. After each correlation step, spurious vectors are identified by universal outlier detection [10] and replaced using linear interpolation. Intermediate vector volumes are filtered before the next iteration by Gaussian smoothing. The final three iterations are performed with an interrogation volume size of $16 \times 16 \times 16$ voxels with a 75% overlap, resulting in a vector spacing of 0.33 mm (4 voxels). Each final volume contains about 7 particles.

Based on comparison to solonoidal filtered results, the uncertainty of the obtained velocity values from 2-frame correlation is estimated to be smaller than 0.5 voxel displacement. The uncertainty estimate for the FTC-based velocity is about 0.1 voxel lower.

The instantaneous pressure is obtained via the momentum equation for inviscid flow (eq. 1).

$$\nabla p = -\rho \frac{Du}{Dt} \quad (1)$$

where p is the static pressure, ρ the density and Du/Dt the material acceleration which is obtained from the PIV velocity data as the slope of a 1st-order least-square fit through velocities along imaginary particle tracks (see [11, 12]). Tracks are calculated over 15 snapshots based on the relation between track length and resulting global pressure fluctuations (see Fig. 2). A iterative integration procedure is employed while ensuring that the CFL condition is met throughout the domain. Equation (1) is then solved for pressure by first casting it into a Poisson equation (see e.g. [13]), which is then discretized using a second-order finite difference scheme. Pressure gradients are prescribed as Neumann boundary conditions on all sides of the domain except for the top. There the mean pressure as obtained from the isentropic flow relation (Bernoulli equation) is prescribed as Dirichlet boundary condition. The resulting linear system is solved using the Matlab algorithm *mldivide*.

3. Results

Results include an investigation of mean flow topology, mean pressure distribution (Figure 3), turbulence intensity and distribution of pressure fluctuations (Figure 4). PIV-based results are validated by comparison to static pressure sensor/microphone measurements and literature. Comparison showed the need for applying a low-pass filter to the PIV-based pressure signal.

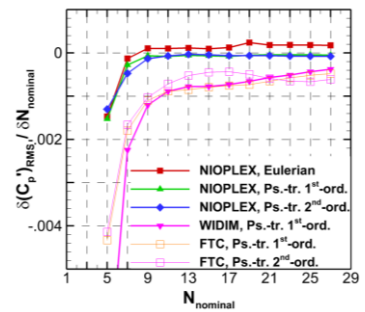


Fig. 2. Change in pressure fluctuations with track length

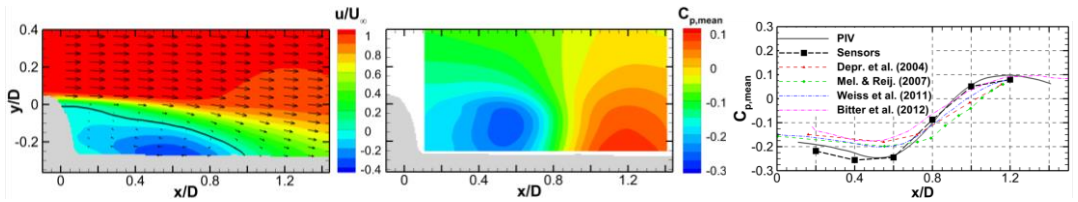


Fig. 3. Mean streamwise velocity (left), mean pressure in fov (centre) and on the afterbody (left)

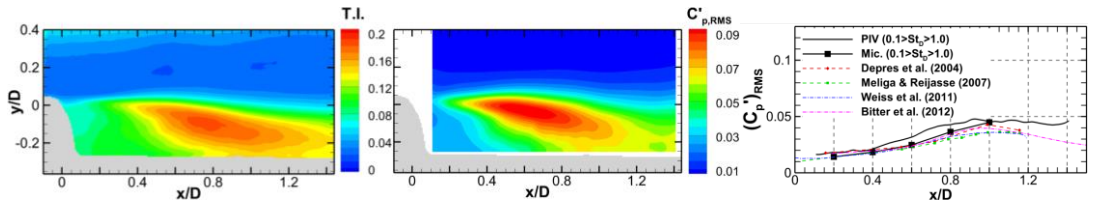


Fig. 4. Turbulence intensity (left), pressure fluctuations in fov (centre) and on the afterbody (left)

Further comparison of the instantaneous PIV-based pressure values to the microphone signal showed reasonable agreement (Figure 5). Cross-correlation yielded normalised correlation coefficients up to 0.8 depending on the cut-off frequency of the low-pass filter and microphone (Figure 6).

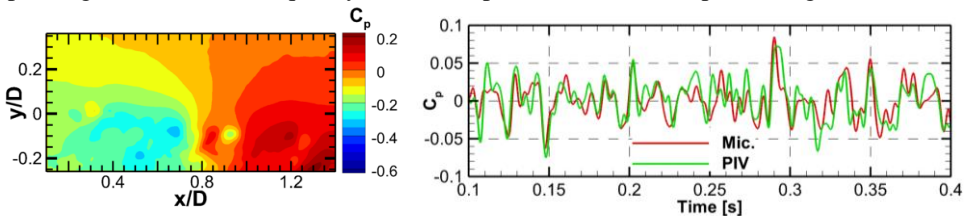


Fig. 5. Example of instantaneous PIV-based pressure field (left) and comparison to microphone signal (right)

A spectral analysis of the PIV and microphone pressure signals was performed to investigate the dependence of the agreement on the chosen frequency band. The coherence (Figure 6) and power spectra (Figure 7) showed a reasonable agreement for frequencies $St_D < 1.0$. For higher frequencies the PIV signal contains mainly noise, which is attributed to the lack of spatial and temporal resolution of the PIV processing and pressure reconstruction. The poor frequency response for $St_D > 1.0$ is in agreement with guidelines proposed by [13]. A clear cut-off frequency of the PIV-signal can be identified at $St_D = 3.0$, which corresponds to the number of snapshots used in the pseudo-tracking approach.

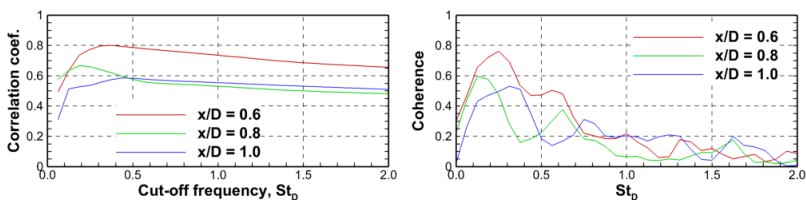


Fig. 6. Normalised cross-correlation coefficient between PIV and microphone pressure signal (left) and coherence (right)

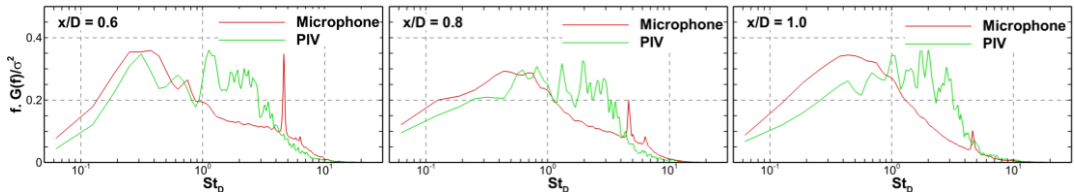


Fig. 7. Estimated normalised power spectral density of microphone and PIV pressure signals

4 Conclusions

Time-resolved, tomographic PIV measurements downstream an axisymmetric step were used to reconstruct instantaneous pressure fields. Validation was provided by comparison to static pressure measurements microphone measurements and literature. Instantaneous PIV results showed reasonable agreement with microphone signals for frequencies $St_D < 1.0$. Depending on the low-pass filtering applied, cross-correlation coefficients reached values up to 0.8. Poor agreement for frequencies $St_D > 1.0$ could be related to poor spatial and temporal resolution. Future work focusses on providing a broader theoretical basis for quantifying the frequency response of PIV-based pressure reconstruction and uncertainty of the obtained results for different implementations of the approach.

5. Acknowledgements

This work is supported by the European FP-7 project “NIOPLEX”, grant agreement 605151.

6. References

1. van Oudheusden BW (2013) PIV-based pressure measurement. *Meas Sci Technol* 24:032001. doi: 10.1088/0957-0233/24/3/032001
2. Scarano F (2013) Tomographic PIV: principles and practice. *Meas Sci Technol* 24:012001. doi: 10.1088/0957-0233/24/1/012001
3. Schanz D, Gesemann S and Schröder A (2016) Shake-The-Box: Lagrangian particle tracking at high particle image densities. *Exp Fluids* 57:70. doi: 10.1007/s00348-016-2157-1
4. Blinde PL, Michaelis D, van Oudheusden BW, Weiss P-E, de Kat R, Laskari A, McPhaden C, Neeteson NJ, Rival DE, Schneider JFG and Schrijer FFJ (2016) Comparative assessment of PIV-based pressure evaluation techniques applied to a transonic base flow. 18th Int. Symp. Appl. Laser Imaging Tech. to Fluid Mech..
5. Wieneke B (2008) Volume self-calibration for 3D particle image velocimetry. *Exp Fluids* 45:549–556. doi: 10.1007/s00348-008-0521-5
6. Atkinson C and Soria J (2009) An efficient simultaneous reconstruction technique for tomographic particle image velocimetry. *Exp Fluids* 47:553–568. doi: 10.1007/s00348-009-0728-0
7. Lynch KP and Scarano F (2013) A high-order time-accurate interrogation method for time-resolved PIV. *Meas. Sci. Technol.* 24, 35305. doi: 10.1088/0957-0233/24/3/035305
8. Scarano, F and Riethmuller, ML (2000), Advances in iterative multigrid PIV image processing. *Exp. Fluids.* 29, S051–S060. doi: 10.1007/s003480070007
9. Discetti S, Natale A and Astarita T (2013) Spatial filtering improved tomographic PIV. *Exp. Fluids.* 54, 1505. doi: 10.1007/s00348-013-1505-7
10. Westerweel J and Scarano F (2005) Universal outlier detection for PIV data. *Exp Fluids* 39:1096–1100. doi: 10.1007/s00348-005-0016-6
11. Pröbsting S, Scarano F, Bernardini M and Pirozzoli S (2013) On the estimation of wall pressure coherence using time-resolved tomographic PIV. *Exp. Fluids.* 54, 15 doi: 10.1007/s00348-013-1567-6

12. Jeon, YJ, Earl T, Braud P, Chatellier L and David L (2016) 3D pressure field around an inclined airfoil by tomographic TR-PIV and its comparison with direct pressure measurements. 18th Int. Symp. Appl. Laser Imaging Tech. to Fluid Mech.
13. de Kat R and van Oudheusden BW (2012) Instantaneous planar pressure determination from PIV in turbulent flow. *Exp Fluids* 52:1089–1106. doi: 10.1007/s00348-011-1237-5
14. Weiss P-E and Deck S (2011) Control of the antisymmetric mode ($m=1$) for high Reynolds axisymmetric turbulent separating/reattaching flows. *Phys Fluids* 23:095102. doi: 10.1063/1.3614481
15. Bitter M, Hara T, Hain R, Yorita D, Asai K and Kähler CJ (2012) Characterization of pressure dynamics in an axisymmetric separating/reattaching flow using fast-responding pressure-sensitive paint. *Exp. Fluids*. 53 doi: 10.1007/s00348-012-1380-7
16. Deprés D, Rejjasse P and Dussauge JP (2004) Analysis of unsteadiness in afterbody transonic flows. *AIAA J.* 42. dor: 10.2514/1.7000
17. Meliga P and Rejjasse P (2007) Unsteady Transonic Flow Behind An Axisymmetric Afterbody Equipped With Two Boosters. 25th AIAA Applied Aerodynamics Conference. American Institute of Aeronautics and Astronautics. doi: 10.2514/6.2007-4564